Geophys. Astrophys. Fluid Dynamics, Vol. 79, pp. 239–257
Reprints available directly from the publisher
Photocopying permitted by license only

DYNAMOS IN WEAKLY CHAOTIC TWO-DIMENSIONAL FLOWS

Y. PONTY, A. POUQUET and P. L. SULEM

CNRS URA 1362, Observatoire de la Côte d'Azur, B.P. 229, 06304 Nice Cedex 04, France

(*Received 1 September 1994; in final form 3 January 1995*)

The dynamo action of a time-periodic two-dimensional flow close to integrability is analyzed. At fixed Reynolds number R^M and frequency ω, magnetic structures develop in the form of both eddies and filaments. The growth rate of the eddies appears to be the same for all frequencies and decreases with R^M, while the growth rate of the filaments displays a strong ω-dependence and, except in the limit of zero or infinite frequencies, converges to a non-zero value as $R^M \to \infty$. Magnetic filaments develop in the widest chaotic zones located near the homoclinic or heteroclinic tangles, and their growth rate is strongly influenced by the width of these zones which is estimated using Melnikov formalism. This study illustrates quantitatively that not only a local stretching but also a sizable chaotic zone is required for fast dynamo action.

KEY WORDS: Fast dynamos, chaotic flows, Melnikov method.

1. INTRODUCTION

Dynamo action in electrically conducting fluids is often considered as the basic mechanism at the origin of the magnetic field in astro and geophysical objects. In the situation where the magnetic Reynolds number R^M is large, the growth rate of a seed magnetic field often appears to be related to the advection rather than the diffusion time scale. This provided a main motivation for efforts devoted to the problem of existence of "fast dynamos" (Vainstein and Zeldovich, 1972) which persist in the limit $R^M \to \infty$, [see Childress (1992) for a recent review]. It was often conjectured, and recently proved in the case of spatially smooth underlying flows (Vishik, 1992; Klapper and Young, 1994), that fluid trajectories are to be chaotic (Lagrangian chaos) for existence of a fast dynamo. Definite evidences of fast dynamos are mostly restricted to discrete flow models (mappings) (Bayly and Childress, 1988; Finn and Ott, 1988; Gilbert, 1992), or to velocity fields displaying singularities (Soward, 1987). The understanding is more limited in the case of smooth flows. A possible candidate is the steady three-dimensional ABC flow (Dombre *et al.*, 1986), but the range of magnetic Reynolds numbers for which the magnetic growth rate was seen to be almost constant, is insufficient to conclude unambiguously (Arnold and Korkina, 1983; Galloway and Frisch, 1986). An explicit example of the spatial structure of the magnetic field resulting from a chaotic dynamo was given by Oseledets (1993).

Examples of flows that seem well-suited for probing the large magnetic Reynolds number limit depend on two space coordinates but are unsteady (Galloway and

Proctor, 1992; Otani, 1993). In this context, magnetic field modes with a different wavevector component in the third direction evolve independently. Consequently, a specific value for this component can be prescribed and the magnetic field computed using a two-dimensional code. An analytical estimate of the growth rate was recently derived for a flow obtained by pulsing two distinct Beltrami waves (Soward, 1993), but the problem of the exchange of the limits (infinite Reynolds number and vanishing transition time between the pulses) remains open. In the case of time-continuous flows $\mathbf{u} = (u_x, u_y, u_z)$, convincing numerical evidence of fast dynamo action was obtained by numerical simulations at magnetic Reynolds numbers up to 10^4 of the so called "circularly polarized model" (CP) (Galloway and Proctor, 1992)

$$\begin{aligned} u_x &= A \sin(z + \varepsilon \sin \Omega t) + C \cos(y + \varepsilon \cos \Omega t), \\ u_y &= A \cos(z + \varepsilon \sin \Omega t), \\ u_z &= C \sin(y + \varepsilon \cos \Omega t), \end{aligned} \tag{1.1}$$

which can be viewed as a time-dependent perturbation of the Robert cellular flow (Robert, 1972). In the present paper, we concentrate on the dynamo action of the CP flow in the regime when the perturbation is assumed to be weak (small ε). The regions of chaos for the underlying dynamical system are then confined near the heteroclinic (when $A = C$) or homoclinic (when $A \neq C$) orbits of the Robert flow. The main issues concern the sensitivity of the dynamo growth rate to the degree of the chaos of the underlying flow and the geometry of the emerging magnetic field, when the flow parameters are varied. Preliminary investigations of the case $A = C$, were reported in Ponty *et al.* (1993).

2. THE CP FLOW

The fluid trajectories of the CP flow, to be understood mod 2π, obey

$$\begin{aligned} \dot{y} &= A \cos(z + \varepsilon \sin \Omega t), \\ \dot{z} &= C \sin(y + \varepsilon \cos \Omega t), \end{aligned} \tag{2.1}$$

together with

$$\dot{x} = A \sin(z + \varepsilon \sin \Omega t) + C \cos(y + \varepsilon \cos \Omega t). \tag{2.1a}$$

By dividing (2.1) and (2.1a) by C and rescaling time in the form $\tau = Ct$, it is easily seen that in addition to the perturbation amplitude ε, the dynamical system depends on the reduced frequency $\omega = \Omega/C$ and on the ratio $a = A/C$. In the absence of perturbation ($\varepsilon = 0$), the two-dimensional system (2.1) admits two elliptic stagnation points $(0, \pi/2)$

and $(\pi, 3\pi/2)$, and also two hyperbolic ones $(0, 3\pi/2)$, and $(\pi, \pi/2)$. These latter points are connected by heteroclinic orbits for $a = 1$, while the system displays homoclinic trajectories when $a \neq 1$. For $\varepsilon \neq 0$, the stagnation points rotate with angular velocity ω on circles of radius ε, centered at the stagnation points of the unperturbed system.

Useful insight on the dynamics of system (2.1) is provided by Poincaré sections (stroboscopic views) at times $\tau = 2\pi n/\omega$ with $n \in \mathcal{N}$. Figure 1 displays such sections for $\omega = 0.8$, when $a = 1$ (on the left hand side) and $a = 0.5$ (on the right hand side), with $\varepsilon = 1, 0.5, 0.2$ and 0.1 (from top to bottom). The case $a = \varepsilon = 1$ is closed to the situation considered by Galloway and Proctor (1992) where $\Omega = 1$, $A = C = \sqrt{3/2}$, corresponding to $\omega = 0.8165$. The chaotic regions cover a significant part of the plane for ε of order unity but concentrate near the heteroclinic or homoclinic orbits of the unperturbed system when ε is decreased. For $a = 1$, these regions are connected, and only one initial condition is necessary to generate the pictures, while, for $a \neq 1$, there are two disjoint chaotic regions, when ε is small enough. A non trivial effect on the size of the chaotic zones is obtained by varying the frequency ω of the perturbation. Figure 2 shows the Poincaré section in the (y, z)-plane in the cases $a = 1$ and $a = 0.5$, for $\varepsilon = 0.1$ and various values of the frequency ω. Significant changes in the thickness of the chaotic regions is visible. We observe in the case $a = 0.5$ that the widths of the chaotic regions associated with distinct homoclinic orbits of the unperturbed system may be different. Note in particular the tiny chaotic zone near the "inner" homoclinic orbit when $\omega = 0.6$, and near the "outer" one when $\omega = 1.9$. As suggested by Leonard *et al.* (1987) and by Ottino (1989), the thickness of the chaotic zones can be estimated by the distance between the stable and unstable manifolds resulting from perturbations of homoclinic or heteroclinic trajectories. In the case of nearly integrable flows, this distance can be computed perturbatively using the Melnikov method, an approach often used to test the existence of transverse homoclinic orbits, leading to Smale horse-shoes and chaotic dynamics (Ottino, 1989; Guckenheimer and Holmes, 1983).

As noticed in Ponty *et al.* (1993), the change of variables

$$\begin{aligned} u &= z - \pi/2 + \varepsilon \sin \omega\tau, \\ v &= y + \varepsilon \cos \omega\tau, \end{aligned} \tag{2.2}$$

puts (2.1) in the standard form

$$\dot{\mathbf{U}} = \mathbf{f} + \varepsilon \mathbf{g}, \tag{2.3}$$

for implementation of the Melnikov method (Guckenheimer and Holmes, 1983). Here $\dot{\mathbf{U}} = (u, v)$, $\mathbf{f} = (\sin v, -a \sin u)$ and $\mathbf{g} = (\omega \cos \omega\tau, -\omega \sin \omega\tau)$. To leading order, the distance between the stable and unstable manifolds is given by

$$d(\tau_0) = \varepsilon \frac{M(\tau_0)}{|\mathbf{f}[\mathbf{q}_0(0)]|}$$

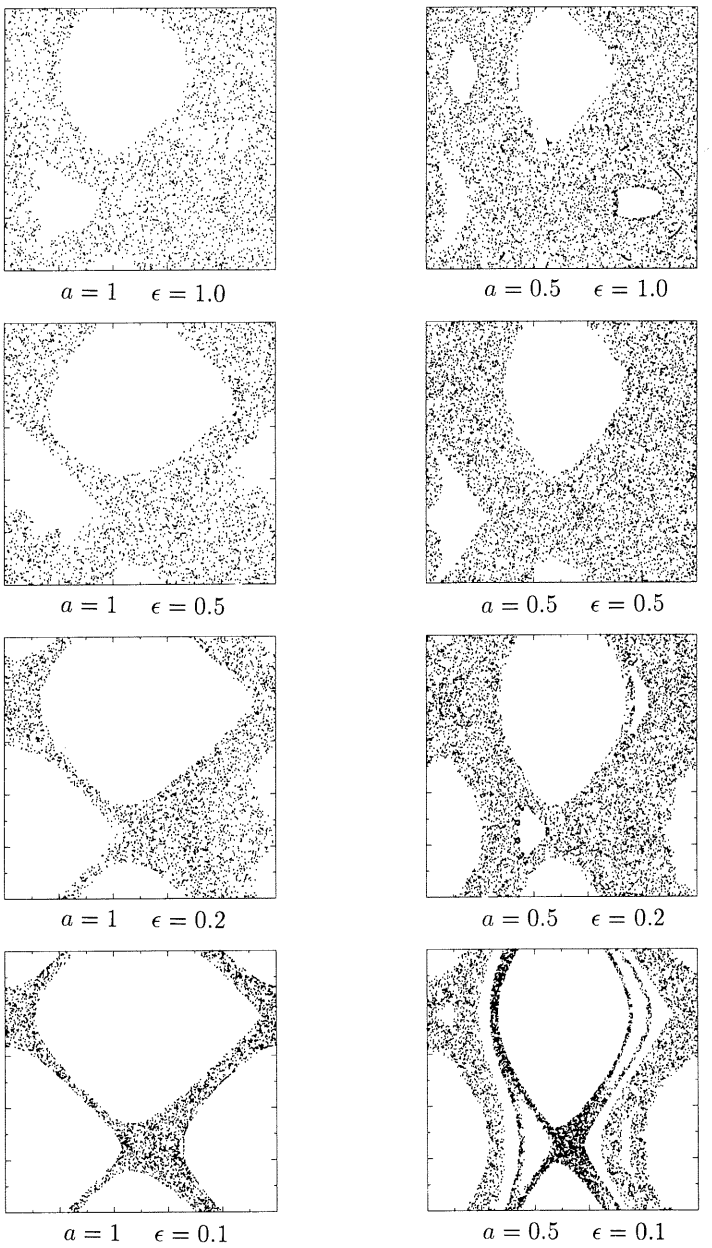

Figure 1 Stroboscopic views at times $t = 2\pi n/\omega$ of the fluid trajectories in a 2π-periodic box of the underlying flow (2.1) with $a = A/C = 1$ (left) and $a = A/C = 0.5$ (right) for different amplitudes ε of the time periodic perturbation, when the reduced frequency is $\omega = \Omega/A = 0.8$.

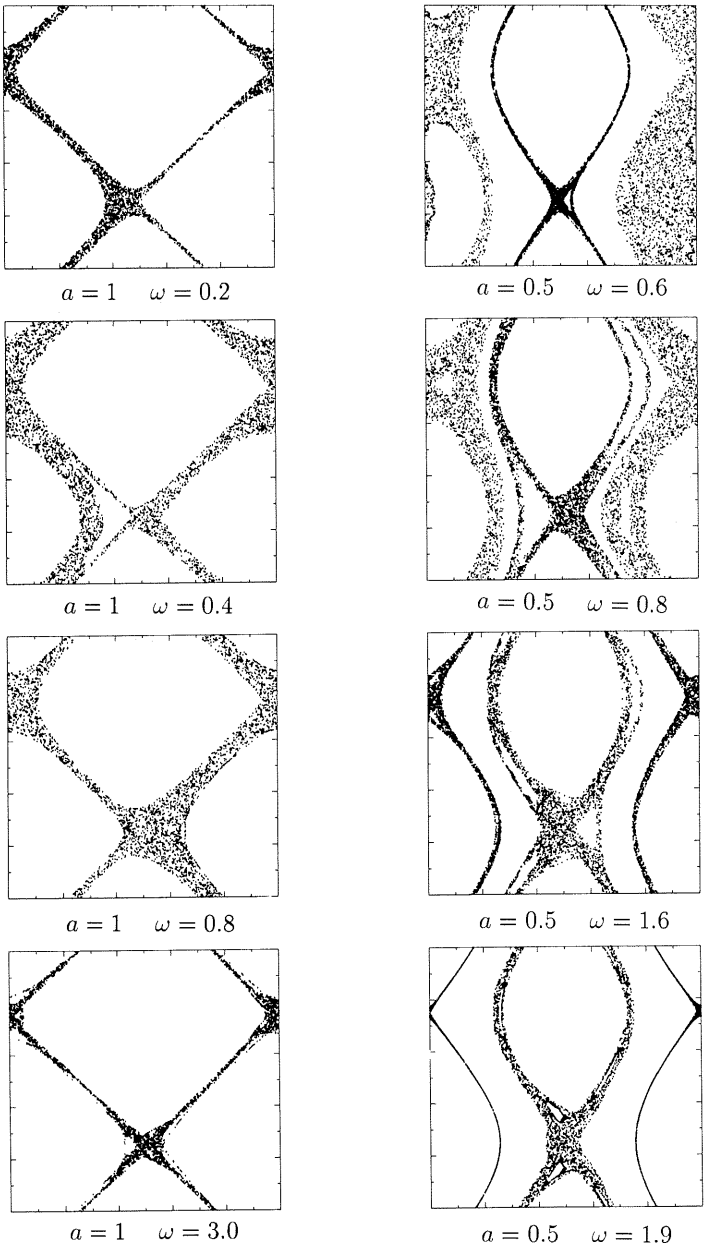

Figure 2 Same stroboscopic views as in Figure 1 with $\varepsilon = 0.1$ and various ω, for $a = 1$ (left) and $a = 0.5$ (right).

with

$$M(\tau_0) = \int_{-\infty}^{\infty} \mathbf{f}[\mathbf{q}_0(\tau)] \times \mathbf{g}[\mathbf{q}_0(\tau), \tau + \tau_0]\, d\tau, \tag{2.4}$$

where $\mathbf{q}_0(t)$ denotes the (unperturbed) homoclinic or heteroclinic orbit. When $\mathbf{q}_0(0)$ is taken at finite distance of the hyperbolic fixed point, $|\mathbf{f}[\mathbf{q}_0(0)]|$ is of order unity.

For $\varepsilon = 0$, the system (2.1) admits four homoclinic or heteroclinic orbits, $\mathbf{q}_0^j = (u_0^j, v_0^j)$, labelled by the subscript j. For each of them, (2.4) becomes

$$M^j(\tau_0) = -\omega \int_{-\infty}^{\infty} \sin v_0^j(\tau) \sin[\omega(\tau + \tau_0)]\, d\tau + a\omega \int_{-\infty}^{\infty} \sin u_0^j(\tau) \cos[\omega(\tau + \tau_0)]\, d\tau. \tag{2.5}$$

For $a = 1$, the chaotic regions are connected and in this case we are mostly interested in the function $F(\omega) = \sup_j \sup_{\tau_0} |M^j(\tau_0)|$ referred to as the "Melnikov function". As shown in Ponty *et al.* (1993), for $a = 1$, we have $F(\omega) = \omega\pi$ sech $(\pi\omega/2)$, a quantity plotted in Figure 3a.

In the case $a \neq 1$, the system displays two distinct chaotic zones for small enough ε. The Melnikov functions associated to each of these zones are computed in the Appendix and plotted in Figure 3b. Note the existence of several zeros and local maxima. The existence of tiny chaotic zones visible in Figure 2 clearly corresponds to the very small value of the associated Melnikov functions.

Another important characteristic of a chaotic system is provided by the Lyapunov exponents and in particular the largest one L which estimates the maximum rate of stretching of the magnetic field. The variation of L for $a = 1$, is plotted as a function of ε, when $\omega = 0.8$ in Figure 4a, and as a function of ω for $\varepsilon = 0.1$ in Figure 4b. We observe that at fixed ω, the largest Lyapunov exponent (like the area of the chaotic zone) tends to saturate when ε is increased. Furthermore, its variation with ω when $\varepsilon = 0.1$ shows that for ω close to 3 or larger (for which the chaotic zones are very small), L remains significant, indicating an important but localized stretching of the magnetic field. A similar result holds when $a \neq 1$. In this case, the chaotic zones are not connected and different but close values are obtained for the Lyapunov exponents of trajectories lying in distinct chaotic regions.

3. DYNAMO GROWTH RATES

Two series of numerical integrations of the induction equation

$$\partial_t \mathbf{b} = \nabla \times (\mathbf{u} \times \mathbf{b}) + \frac{1}{R^M} \Delta \mathbf{b}, \tag{3.1}$$

have been performed with the velocity field (2.1), one with $A = C = \sqrt{3/2}$ (corresponding to $a = 1$) and the other with $A = C/2 = \sqrt{3/5}$ (for which $a = 0.5$). In both series of

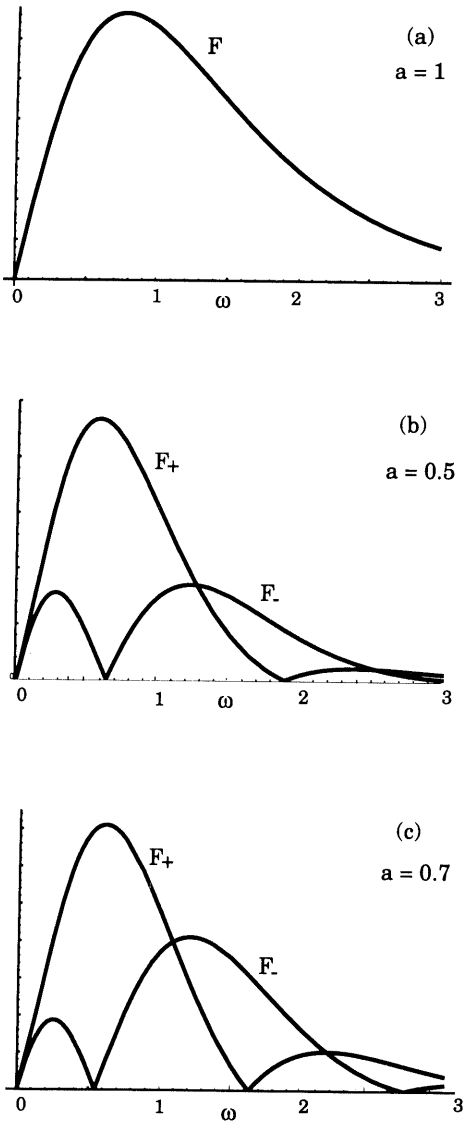

Figure 3 (a) The Melnikov function for $a = 1$; (b) Melnikov functions F_+ and F_- associated to the outer and inner chaotic zones respectively, for $a = 0.5$. (c) Melnikov functions F_+ and F_- for $a = 0.7$.

runs, the parameters ε and ω are varied. We concentrate on magnetic fields with a wavevector component in the x-direction $k_1 = 0.57$, as in Galloway and Proctor (1992). Furthermore, the velocity field (1.1) including only Fourier modes of wavenumber unity, the induction equation is efficiently solved in the spectral space, since in this case, the convolutions require, for each direction, a number of operations equal to the number of retained modes. We observe that as R^M exceeds a critical value of order of

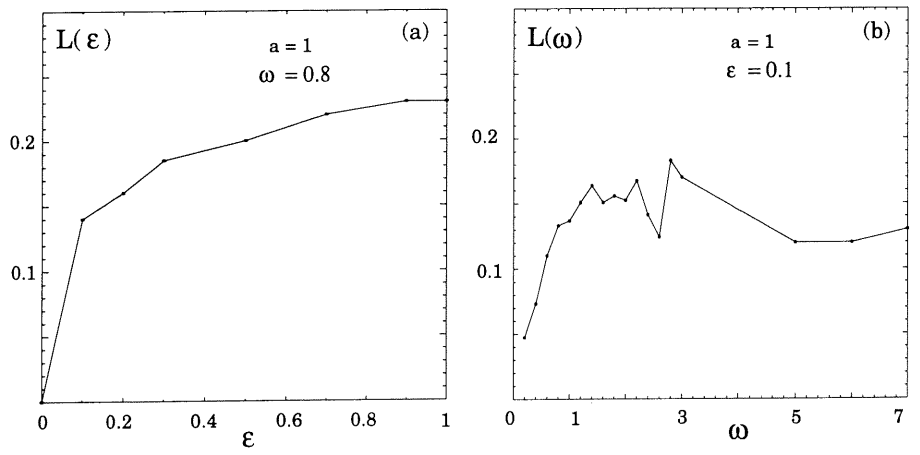

Figure 4 Largest Lyapunov exponent L for $a = 1$: (a) versus ε for $\omega = 0.8$; (b) versus ω for $\varepsilon = 0.1$.

a few units (depending on the velocity field parameters), a dynamo action takes place and, after a transient, the magnetic energy $E^M = \int |B|^2 \, d\mathbf{x}$ grows exponentially. This "kinematic dynamo" where the flow motion is given, models the early time amplification of a seed magnetic field. Later on, the magnetic field usually reacts on the flow through the Lorentz force, leading to a saturation of the dynamo, a question which is beyond the object of the present paper.

We are here mainly interested in the influence of the velocity parameters on the dynamo growth rate $\lambda = \lim_{t\to\infty} (1/2t) \ln E^M$. Special attention is devoted to the limit $R^M \to \infty$, an asymptotic regime which is approached non uniformly, and requires larger Reynolds numbers as ε is decreased. The influence of the deviation from integrability of the underlying flow is illustrated in Figure 5a which displays the variation of λ with ε, for $a = 1$, $\omega = 0.8$ and $R^M = 500$. For comparison, the variation of the relative area S of the chaotic zones in the $(y - z)$-plane is plotted in Figure 5b. A strong correlation between the two quantities is visible, although the Reynolds number is moderate.

In the context of a fast dynamo, an important issue is the variation of the growth rate λ with the magnetic Reynolds number R^M. Figure 6 shows this variation for $a = 1$ and different values of the perturbation frequency ω within the intervals (a) $0.2 \leqslant \omega \leqslant 0.8$ and (b) $0.8 \leqslant \omega \leqslant 3.0$. For low Reynolds numbers, the growth rate is essentially independent of ω, whereas a non trivial dependency emerges when R^M exceeds a few tens. The maximal growth rate occurs near $\omega = 0.8$. At this frequency, a tendency of λ to saturate is seen when the Reynolds number reaches values of order 10^4. Such large values of R^M are required because of the smallness of ε (here equal to 0.1). In the case $\varepsilon = 1$ and ω close to 0.8 considered by Galloway and Proctor (1992), convergence was obtained with $R^M \sim 100$. Furthermore, at both low and high frequencies within the considered range, we observe an intermediate domain of Reynolds numbers for which λ is independent of ω and decreases with R^M. At higher Reynolds numbers (depending

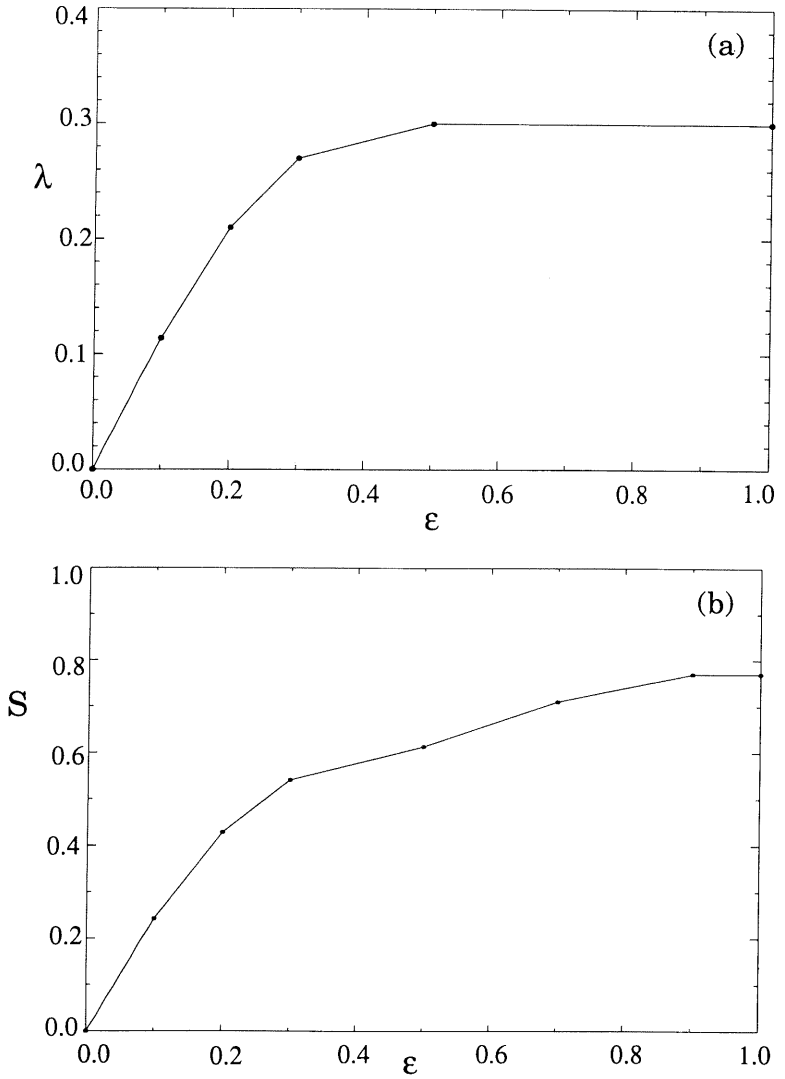

Figure 5 (a) Magnetic field growth rate λ versus ε for $a = 1, \omega = 0.8$ and $R^M = 500$. (b) Variation with ε of the fraction S of the $(y-z)$-domain associated with a chaotic dynamics for $\omega = 0.8$.

on ω), a different behavior is observed: the growth rate increases with R^M and shows a tendency to saturate at a finite value, indicative of a fast dynamo. The Reynolds numbers we used seem insufficient to approach this asymptotic regime when $\omega > 1.6$.

The variation of the growth rate λ with ω for the simulations at the largest available magnetic Reynolds numbers is conveniently presented in Figure 7. For both small and large values of ω, plateaux whose amplitude decreases with R^M, are visible. At moderate

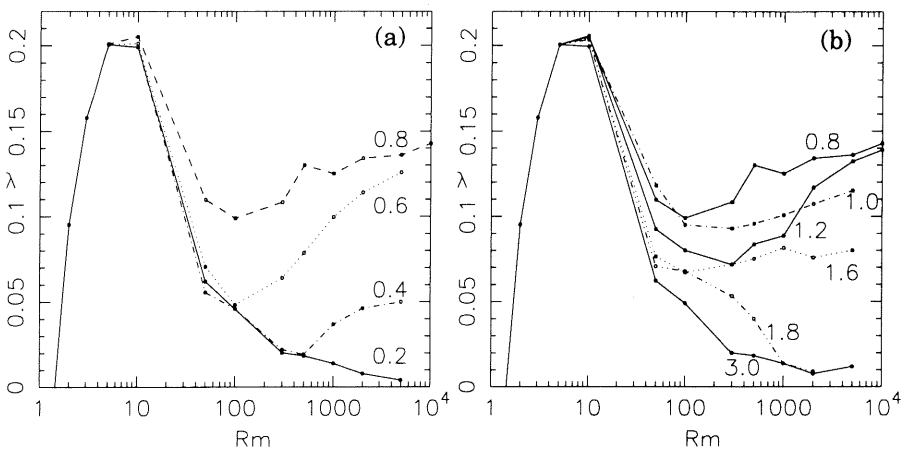

Figure 6 Magnetic field growth rate λ versus the magnetic Reynolds number R^M for $a = 1$ and $\varepsilon = 0.1$. Curves are labelled by the corresponding values of ω.

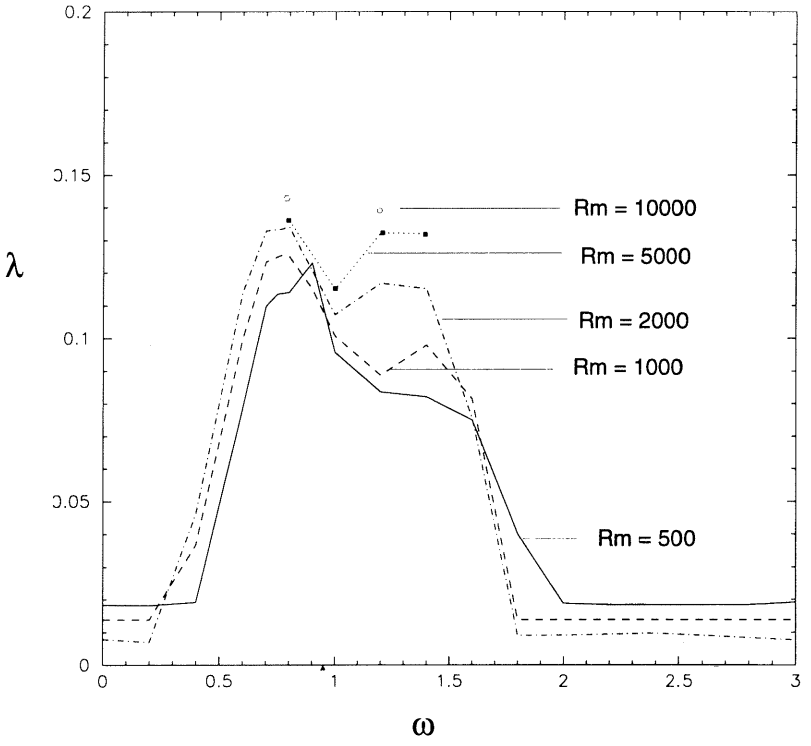

Figure 7 Magnetic field growth rate versus ω for several Reynolds numbers ($\varepsilon = 0.1$).

Reynolds numbers, two maxima are present near $\omega = 0.8$ and $\omega = 1.4$, and tend to get nearer as R^M is increased. This picture of bumps and plateaux suggests that two types of dynamos are operating in such flows. For values of the perturbation frequency ω near unity, the convergence of the magnetic field growth rate as the Reynolds number is increased, indicates the existence of a fast dynamo. As seen on Figure 5, the presumed asymptotic growth rate for $\omega = 0.8$ and $\varepsilon = 0.1$ is about 0.11, roughly one third of the value gives by Galloway and Proctor (1992) for $\varepsilon = 1$. On the other hand, the two plateaux are indicative of a slow dynamo, at least if the behavior we observe can be extrapolated to infinite Reynolds numbers.

When analyzing the influence of the frequency ω on the dynamo efficiency, we note for the case of small ε (Figure 7), the proximity of the largest magnetic field growth rate and the maximum of the Melnikov function (Figure 3a). In contrast, this frequency range is by no way singled out for the largest Lyapunov exponent (Figure 4). This suggests that, at least for weakly chaotic systems (small ε), the width of the chaotic zones has a dominant influence on the efficiency of the dynamo action. An estimate of the magnetic growth rate was proposed by Ott *et al.* (1992) and Du and Ott (1993) in terms of Lyapunov exponents, and of the cancellation exponent which characterizes the complexity of the small-scale structure of the emerging magnetic field. A measure of this exponent requires huge Reynolds numbers, several orders of magnitudes in excess of those used in the present simulations where, as seen in Figure 12, individual magnetic field lobes are well-resolved but scanty.

In the case $a = 0.5$, for which heteroclinic connections are replaced by homoclinic orbits in the unperturbed underlying flow, Figure 8 shows the growth rate λ versus ω at Reynolds number $R^M = 500$, for $\varepsilon = 0.1$ and 0.2. In the latter case, chaotic zones in the Poincaré section which are distinct for $\varepsilon = 0.1$ have merged (see Figure 1) and the growth rate remains significant on a more extended range of frequencies. Although the Reynolds number is moderate, the growth rate appears to be again dominant near $\omega = 0.8$, not far from the maximum $\omega = 0.6$ of the largest Melnikov function (Figure 3b), and this for both values of ε.

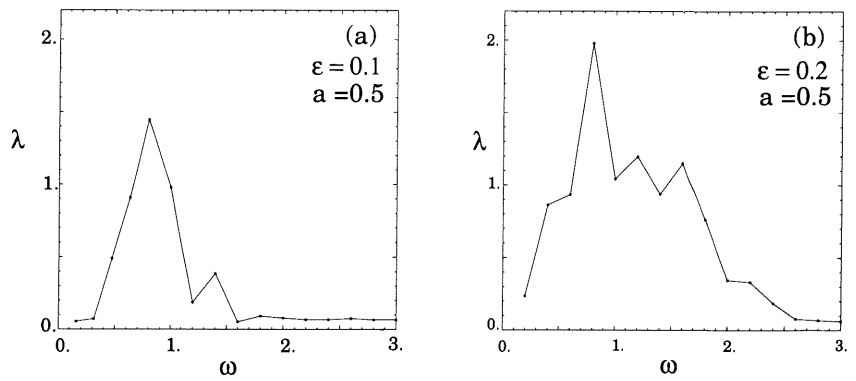

Figure 8 Growth rate λ versus ω at Reynolds numbers $R^M = 500$, for $a = 0.5$, (a) when $\varepsilon = 0.1$ (a) and (b) $\varepsilon = 0.2$ (b).

4. GEOMETRY OF THE MAGNETIC FIELD

Figure 9 shows for $a = 1$, $\varepsilon = 0.1$ and various values of the frequency ω, the contours of the magnetic field strength $|b|$ in the plane $x = 0$, when the exponential growth is well established. Figure 10 presents similar results for $a = 0.5$. It is clear from both figures that two types of structures have emerged. Roundish magnetic eddies are dominant for both low and high values of ω, whereas elongated filaments dominate for values of ω near the maximum growth rate. Eddies are localized in the vicinity of elliptic stagnation points, while filaments are concentrated in the immediate neighborhood of

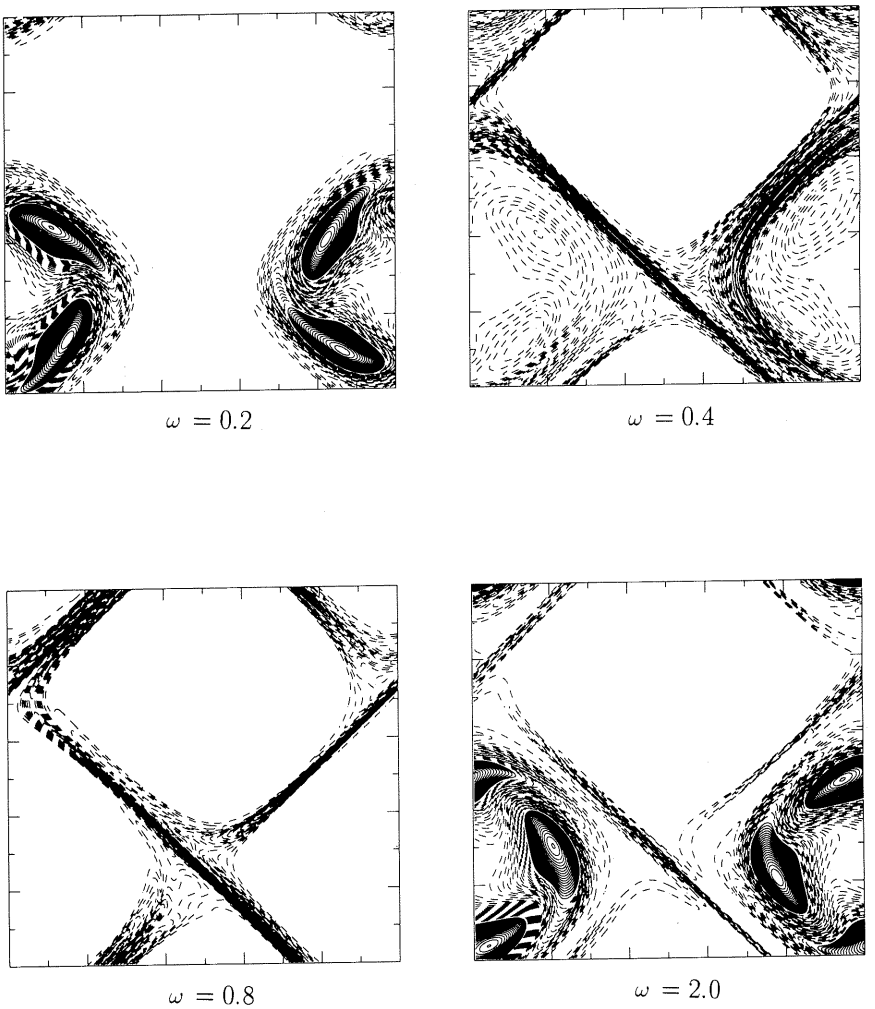

Figure 9 Magnetic contours for $a = 1$, $\varepsilon = 0.1$, $R^M = 2000$ and various ω.

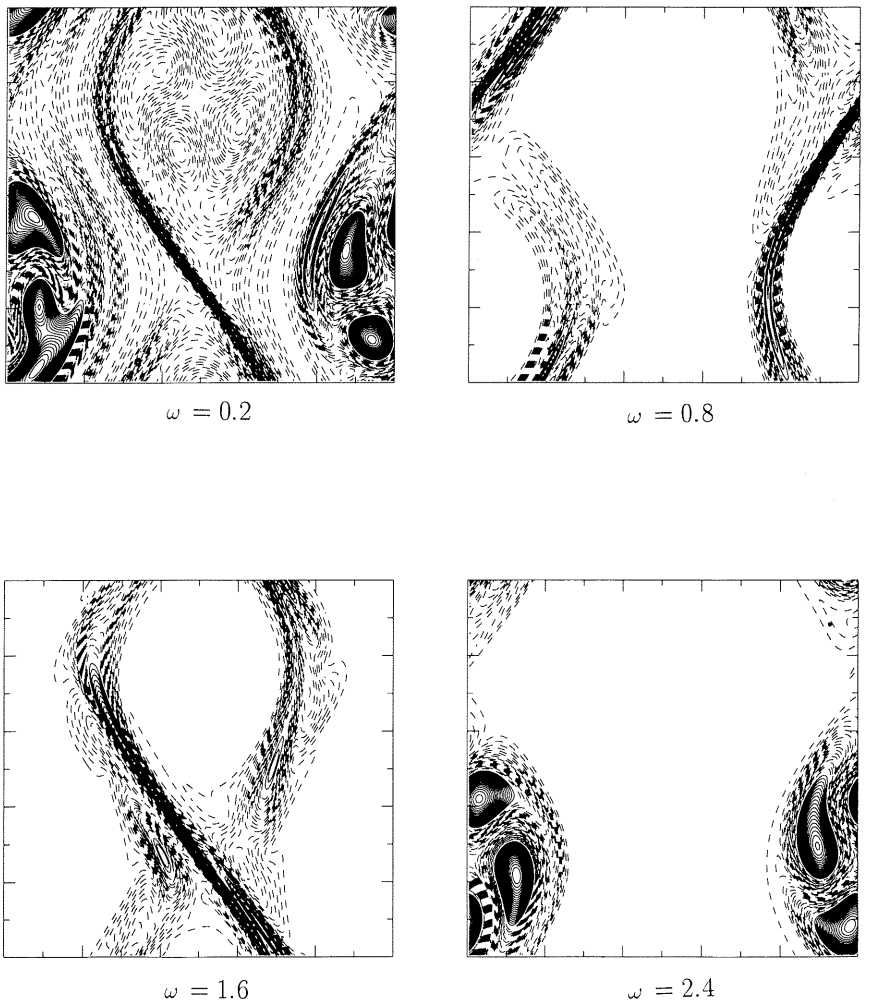

Figure 10 Magnetic contours for $a = 0.5$, $\varepsilon = 0.1$, $R^M = 2000$ and various ω.

the unstable manifolds of the hyperbolic stagnation points with the peak field centered close to them.

The three-dimensional perspectives displayed in Figure 11 for $a = 1$, show that the eddies are associated with magnetic fields transverse to the (y, z)-plane and pointing in opposite directions. The filaments are mostly contained within the (y, z)-plane, and as the Reynolds number is increased, the magnetic field modulus displays more spatial oscillations in the transverse direction (Figure 12). The relative importance of the eddies and the filaments may depend on time, since their growth rates are different. A quantitative measurement was made for $a = 1$, $\varepsilon = 0.1$ and $R^M = 500$. For all tested values of the frequency ω, the growth rate of the eddies remains essentially constant and close to 0.02, whereas the filament growth rate (which strongly depends on ω)

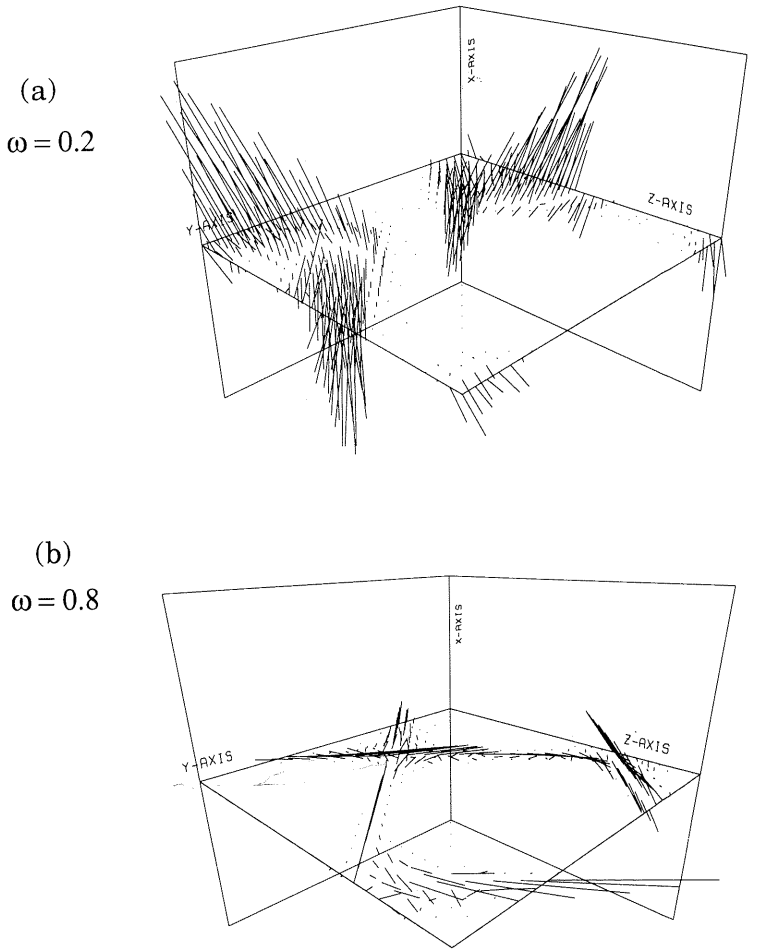

Figure 11 Three-dimensional perspective view of the magnetic field when $a = 1$ and $R^M = 500$. (a) for $\omega = 0.2$, (b) for $\omega = 0.8$,

dominates, except possibly for very small and very large ω. The lack of dependence on ω of the eddy growth rate is at the origin of the plateaux displayed in Figure 7, which were seen to decrease with R^M, a characteristic property of a slow dynamo. In contrast, the filaments seem associated to fast dynamo action.

The spectral signatures of the two types of spatial structures is visible in Figure 13 where, as can be seen, the magnetic energy spectra is plotted in lin-log coordinates for the parameters $a = 1$, $\varepsilon = 0.1$, $R^M = 5000$ with (a) $\omega = 0.8$ and (b) $\omega = 0.2$. In the former case, the spectrum is quasi-constant up to $k \sim 50$, corresponding to a sharp structure of width $\delta l \sim 2\pi/50$ (see Figure 12). In the latter, the spectrum decreases rapidly, until it meets (at a level of order 10^{-10}) a broad band noisy spectrum corresponding to a low-level filamentary structure with smaller growth rate, as can be checked on contours with logarithmically assigned values.

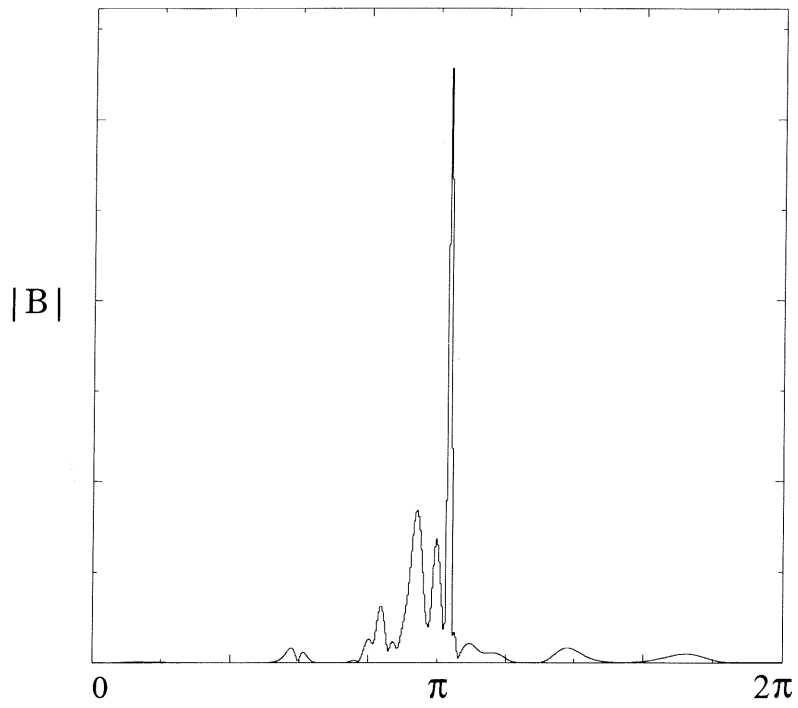

Figure 12 Variation of the magnetic field modulus along $z = \frac{1}{2}\pi$, for $\omega = 0.8$, $a = 1$ and $R^M = 5000$ (linear scale).

When $a \neq 1$ and ε small enough, two distinct chaotic zones exist, as shown in Figure 2. By inspection of Figure 10, it is striking that the fastest growing magnetic structures are localized in space in the wider chaotic regions, as measured by the Melnikov function (Figure 3b). Indeed, for $a = 0.5$, when $\omega = 0.8$, the F_+ function defined in the Appendix is dominant (see Figure 3b) and the magnetic field grows near the perturbed homoclinic orbit associated to the $(0, 3\pi/2)$ stagnation point ("inner orbit"), whereas when $\omega = 1.6$, F_- is dominant and the magnetic field growths near the homoclinic orbit associated to the $(\pi, \pi/2)$-stagnation point ("outer orbit"). We checked that this configuration is preserved when the Reynolds number is increased. Similar observations were made for other values of a (still keeping $\varepsilon = 0.1$). The generated magnetic field which develops for $a = 0.7$ is shown when $\omega = 0.6$ (which as seen in Figure 3c corresponds to a strong dominance of F_+), $\omega = 1.0$ (in which case F_+ and F_- are almost equal), $\omega = 1.5$ (for which F^- is dominant) and finally $\omega = 2.5$ (where F_+ and F_- are both relatively small, although F_+ still dominates). We indeed observe that when F_+ (resp. F_-) dominates, the magnetic field develops in the outer (resp. inner) chaotic region. This determinant influence of the largest Melnikov function was also successfully tested with $a = 0.2$ and $\varepsilon = 0.1$. However, when at fixed ε the value of a is increased (for example $\varepsilon = 0.1$ and $a = 0.8$), the chaotic zones tend to merge and the magnetic field develops in the common chaotic zone.

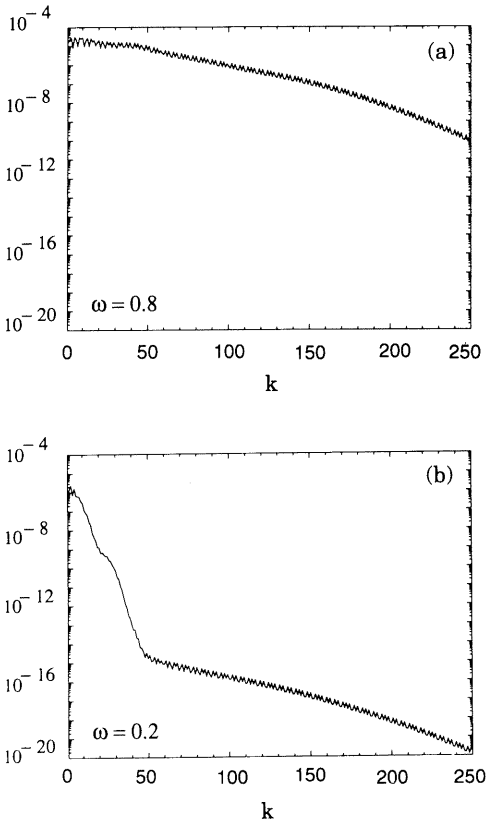

Figure 13 Magnetic energy spectra in lin-log coordinates for $a = 1$, $R^M = 5000$ with (a) $\omega = 0.8$ and (b) $\omega = 0.2$.

Finally, for $a = 0.5$, we observe that when the chaotic zones are no longer distinct (for example $\omega = 0.8$ at $\varepsilon = 0.2$), the dominant magnetic structures (not shown) are still located near the same unstable manifold as in the case $\varepsilon = 0.1$ where the chaotic zones are distinct. This is similar to the observation that for $a = 1$ and $\varepsilon = 1$ (where the chaotic zones are very extended), the magnetic structures develop in the vicinity of the unstable manifold of the hyperbolic point (Galloway and Proctor, 1992).

In conclusion, we have considered the kinematic dynamo action of steady two-dimensional flows subject to weak time-periodic perturbations, thus falling into the realm of almost integrable dynamics for the fluid particles. We observed that different magnetic structures are generated in the integral and chaotic zones. In the latter, magnetic structures in the form of sheets survive in the limit of infinite Reynolds number and appear to be strongly sensitive to the width of the chaotic zones controlled by the time frequency of the flow and quantitatively estimated in the context of the Melnikov theory. An interesting question is the stability of these structures in the full magnetohydrodynamic regime, when the reaction of the Lorentz force on the fluid velocity becomes relevant.

Acknowledgements

The computations were performed on the CRAY YMP of the Institut Méditérranéen de Technologie (Marseille), with computer time provided by the Région Provence-Alpes-Côte d'Azur. Support from the European Cooperative Network "Numerical Simulations of Nonlinear Phenomena" ERBCHRXCT930410 is acknowledged. This work was initiated with V. Rom-Kedar, while she was visiting the Observatoire de Nice.

References

Arnold, V. I. and Korkina, E. I., "The growth of a magnetic field in a three-dimensional steady incompressible flow", *Vestn. Mosk. Univ. Mat. Mekh.* **3**, 43–46 (1983).

Bayly, B. and Childress, S., "Construction of the fast dynamo using unsteady flows and maps in three dimensions," *Geophys. Astrophys Fluid Dynam.* **44**, 221–240 (1988).

Childress, S., "Fast dynamo theory," in: *Topological Aspects of the Dynamics of Fluids and Plasmas*, 111–147, (Eds. H. K. Moffatt, G. M. Zaslavsky, P. Comte and M. Tabor). *NATO ASI series E*, **218**, Kluwer (1992).

Dombre, T., Frisch, U., Greene, J. M., Hénon, M., Mehr, A. and Soward, A. M., "Chaotic streamlines in the ABC flows," *J. Fluid Mech.* **167**, 353–391 (1986).

Du, Y. and Ott, E., "Growth rates for fast kinematic dynamo instabilities of chaotic fluid flows," *J. Fluid Mech.* **257**, 265–288 (1993).

Finn and Ott, E., "Chaotic flows and fast magnetic dynamos," *Phys. Fluids* **31**, 2992–3012 (1988).

Galloway, D. J. and Frisch, U., "Dynamo action in a family of flows with chaotic stream lines," *Geophys. Astrophys. Fluid Dynam.* **36**, 53–83 (1986).

Galloway, D. J. and Proctor, M. R. E., "Numerical calculations of fast dynamos for smooth velocity field with realistic diffusion," *Nature* **356**, 691–693 (1992).

Gilbert, A., "Magnetic field evolution in steady chaotic flows," *Phil. Trans. R. Soc. Lond.* A **339**, 627–656 (1992).

Guckenheimer, J. and Holmes, P., "Nonlinear oscillations, dynamical systems, and bifurcations of vector fields," *Applied Mathematical Sciences* **42**, Springer-Verlag (1983).

Klapper, I. and Young, L. S., "Rigorous bound on the fast dynamo growth rate involving topological entropy," Preprint (1994).

Leonard, A., Rom-Kedar, V. and Wiggins, S., "Fluid mixing and dynamical systems," *Nucl. Phys.* **B** (*Proc. Suppl.*) **2**, 179–190 (1987).

Oseledets, V., "Fast dynamo problem for a smooth map on a two-torus," *Geophys. Astrophys. Fluid Dynam.* **73**, 133–145 (1993).

Otani, N. F., "A fast kinematic dynamo in two-dimensional time dependent flows," *J. Fluid Mech.* **253**, 327–340 (1993).

Ott, E., Du, Y., Sreenivasan, K. R., Juneja, A. and Suri, A. K., "Sign-singular measures: fast magnetic dynamos, and high-Reynolds-number fluid turbulence," *Phys. Rev. Lett.* **69**, 2654–2657 (1992).

Ottino, J. M., *The Kinematics of Mixing: Stretching, Chaos and Transport*, Cambridge Texts in Applied Mathematics, Cambridge University Press (1989).

Ponty, Y., Pouquet, A., Rom-Kedar, A. and Sulem, P. L., "Dynamo action in a nearly integrable chaotic flow," in: *Solar and planetary dynamos* 241–248 (Eds M. R. E. Proctor, P. C. Matthews and A. M. Rucklige) Cambridge University Press (1993).

Robert, G. O., "Dynamo action of fluid motions with two-dimensional periodicity," *Phil. Trans. R. Soc. Lond.* A **271**, 411–454 (1972).

Soward, A. M., "Fast dynamo action in a steady flow," *J. Fluid Mech.* **180**, 267–295 (1987).

Soward, A. M., "An asymptotic solution of a fast dynamo in two-dimensional pulsed flow," *Geophys. Astrophys. Fluid Dynam.* **73**, 179–215 (1993).

Vainshtein, S. I. and Zeldovich, Ya. B., "Origin of magnetic fields in astrophysics," *Usp. Fiz. Nank.* **106**, 431–457 (*Sov. Phys. Usp.* **15**, 159–172) (1972).

Vishik, M. M., (1992) unpublished.

APPENDIX

We compute here the Melnikov functions for the two chaotic zones associated to perturbed homoclinic orbits of the dynamical system (2.1), in the case $a \neq 1$. Due to the system symmetries, it is sufficient to concentrate on $a < 1$. Using the notation of Section 2, the solution (u_0, v_0) of the unperturbed system (2.3) with $\varepsilon = 0$, rewrites

$$d\tau = S_1 \frac{du_0}{\sqrt{1-(H-a\cos u_0)^2}}, \quad d\tau = -S_2 \frac{dv_0}{a\sqrt{1-a^{-2}(H-\cos v_0)^2}}, \tag{A.1}$$

where $H(u_0, v_0) = \cos v_0 + a \cos u_0$ is the associated Hamiltonian. Here $S_1 = \text{sign}(du_0/d\tau)$ and $S_2 = \text{sign}(dv_0/d\tau)$ depend on the direction along which the system evolves on the orbit. The initial conditions corresponding to $u_0 = \pi$ on the branches $j = 1$ and $j = 2$, to $v_0 = 0$ on the branch $j = 3$, $v_0 = 2\pi$ on the branch $j = 4$ (see Figure 14). Concerning the sign of S_1 and S_2, on $j = 1$ for example, we have $S1 = -1$, while $S2 = 1$ for $\tau > 0$ and $S2 = -1$ for $\tau < 0$.

At the "inner" fixed point A corresponding to $(u_0, v_0) = (0, \pi)$ [or $(\pi, \pi/2)$ in the original coordinates], $H = a - 1 < 0$, while at the "outer" fixed point B of coordinates $(\pi, 0)$ [or $(0, 3\pi/2)$ in the original coordinates], $H = 1 - a > 0$.

To deal with (A.1), it is convenient to define $\phi = [\tan(u_0/2)]^S$ and $\psi = \sqrt{a}\,[\tan(v_0/2)]^{-S}$, where $S = \text{sign}(H)$. For the inner orbit, $S = -1$, while for the

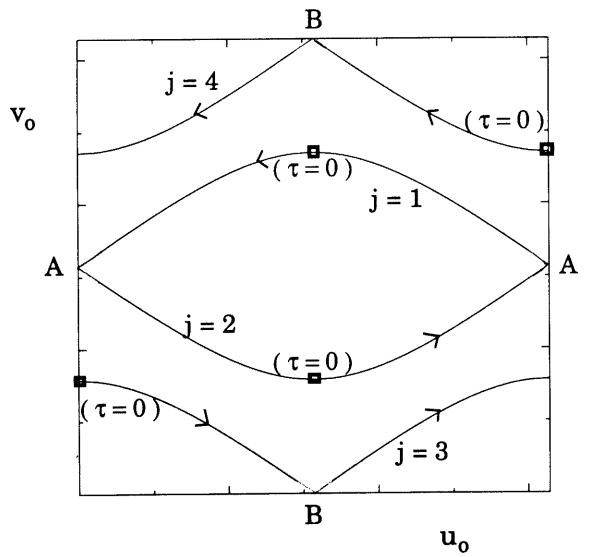

Figure 14 The various homoclinic orbits (indexed by j) for the unperturbed system ($\varepsilon = 0$) with $a = 0.5$. On each orbit, the small square labeled by ($\tau = 0$), indicates the initial conditions used in the analysis presented in the Appendix.

outer orbit $S = 1$. We write

$$\cos u_0 = S\frac{1-\phi^2}{1+\phi^2}, \quad \cos v_0 = -S\frac{a-\psi^2}{a+\psi^2}.$$

Prescribing that at the initial time $\tau_0 = 0$, $\phi(0) = 0$ and $\psi(0) = \sqrt{1-a}$, the solution of (A.1) reads

$$\phi = \sqrt{1-a}\sinh(S S_1 \sqrt{a}\tau)$$

$$\psi = \sqrt{1-a}\cosh(S S_2 \sqrt{a}\tau).$$

This enables us to express

$$\sin u_0 = -S_2\frac{2\phi}{1+\phi^2}, \quad \sin v_0 = S_1\frac{2\sqrt{a}\psi}{(a+\psi^2)}. \tag{A.2}$$

Substituting in (2.5) and computing the resulting integrals with the condition that for $a < 1$, $v_0(\tau) = v_0(-\tau)$ and $u_0(\tau) = -u_0(-\tau)$, we obtain for the Melnikov functions $F_+(\omega)$ and $F_-(\omega)$, associated to outer and inner chaotic zones respectively,

$$F_+(\omega) = \sup_{j=2,3} \sup_{\tau_0} |M^j(\tau_0)| = |(a\omega I_1 + \omega I_2)|$$

and

$$F_-(\omega) = \sup_{j=1,4} \sup_{\tau_0} |M^j(\tau_0)| = |(a\omega I_1 - \omega I_2)|,$$

with

$$I_1 = 4\frac{\sqrt{1-a}}{\sqrt{a}}\int_0^\infty \frac{\sinh t}{1+(1-a)\sinh^2 t}\sin\left(\frac{\omega}{\sqrt{a}}t\right)dt,$$

$$I_2 = 4\sqrt{1-a}\int_0^\infty \frac{\cosh t}{1+(1-a)\sinh^2 t}\cos\left(\frac{\omega}{\sqrt{a}}t\right)dt.$$

These two functions are plotted in Figure 3b for $a = 0.5$. and in Figure 3c for $a = 0.7$.